J. Fluid Mech. (2012), *vol.* 707, *pp.* 541–550.
doi:10.1017/jfm.2012.298

Three-dimensional vortex structure on a rotating wing

Cem A. Ozen and D. Rockwell†

Department of Mechanical Engineering & Mechanics, Lehigh University, Bethlehem, PA 18015, USA

(Received 29 March 2012; revised 4 June 2012; accepted 12 June 2012;
first published online 6 August 2012)

The three-dimensional structure of the leading-edge vortex on a rotating wing is addressed using a technique of particle image velocimetry. Organized patterns of chordwise-oriented vorticity, which exist within the vortex, arise from the spanwise flow along the surface of the wing, which can attain a velocity the same order as the velocity of the wing at its radius of gyration. These patterns are related to the strength (circulation) and coherence of the tip and root vortices. The associated distributions of spanwise-oriented vorticity along the leading-edge vortex are characterized in relation to the vorticity flux and downwash along the wing.

1. Introduction

In recent decades, substantial advances have led to insight into the flow structure on rotating wings. Of specific interest herein are those investigations that explicitly address spanwise flow in relation to existence of a stable leading-edge vortex (LEV). Relevant studies include wings undergoing simultaneous rotation and pitching, and unsteady and steady rotation in the absence of pitching. Qualitative smoke, bubble or dye visualization has been employed by Ellington *et al.* (1996), van den Berg & Ellington (1997), Willmott, Ellington & Thomas (1997), Thomas *et al.* (2004), Lentink & Dickinson (2009) and DeVoria *et al.* (2011). Sectional imaging involving either chordwise or spanwise planes, or a combination of them, has been used by Birch & Dickinson (2001), Birch, Dickson & Dickinson (2004), Ansari *et al.* (2009), Jones, Ford & Babinsky (2011), Ozen & Rockwell (2012) and Wojcik & Buchholz (2012). Volume imaging with interpretation of selected sections has been employed by Liu *et al.* (1998), Poelma, Dickson & Dickinson (2006), Aono, Liang & Liu (2008), Lu & Shen (2008), Kim & Gharib (2010) and Carr *et al.* (2012). These investigations extend over a wide range of Reynolds number, and reveal a number of important phenomena, including a coherent and stable (LEV), possible occurrence of vortex breakdown, the distribution and magnitude of spanwise velocity and the history of the lift acting on the wing. The three-dimensional nature of the major features of the flow structure and the relationships between them are, however, not adequately understood.

The present study employs volume representations to characterize the structure of the LEV, with emphasis on generation of chordwise-oriented vorticity in presence of spanwise flow. The associated states of the tip and root vortices, distributions of spanwise vorticity within the LEV, and downwash along the wing are also determined.

† Email address for correspondence: dor0@lehigh.edu

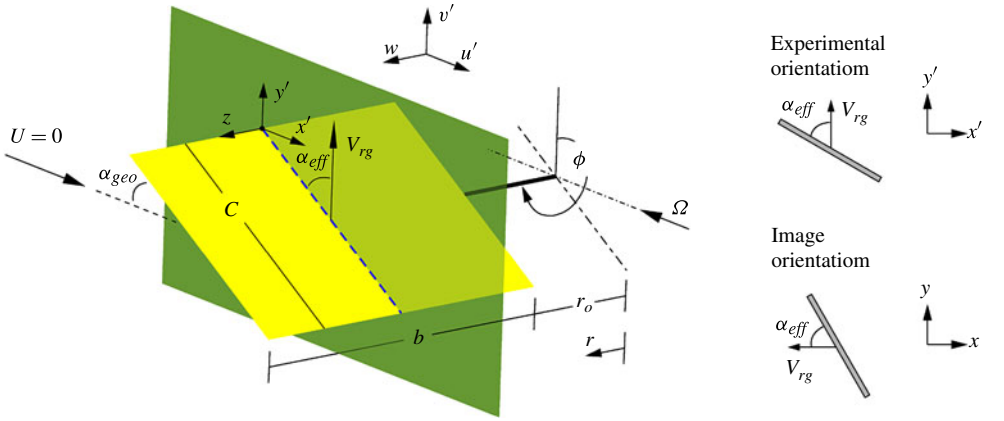

FIGURE 1. Schematic of a rotating wing and related parameters.

2. Experimental system and techniques

Figure 1 shows an isometric view of the wing and related parameters. The colour yellow represents the wing, which has an aspect ratio $AR = 2.05$, a chord $C = 38.1$ mm, a span $b = 78.1$ mm and a thickness $t = 2.8$ mm. It is made from clear Plexiglas and the edges are squared off. The root of the wing is connected to the body of revolution by a rod with diameter 3.2 mm and length 26 mm; the rod is located at the mid-chord of the wing. The diameter of the body of revolution is 12.8 mm and it is rotated in the direction shown in figure 1 at an angular velocity of $\Omega = 5.6$ rad s^{-1}. The radial distance from the axis of rotation is represented by r. It has values of $r_o = 32.5$ mm, $r_g = 71.5$ mm and $r_{tip} = 110.6$ mm at, respectively, the root of the wing, the radius of gyration of the wing (located $1C$ from the root of the wing) and the tip of the wing. The effective angle of attack is $\alpha_{eff} = 45°$ for all experiments. The geometric angle of attack α_{geo} is not relevant, as $U = 0$.

Details of the experimental system are described by Ozen & Rockwell (2012). The rotational motion of the wing starts from rest at $\phi = 0°$, reaches constant velocity at $\phi = 27°$ and ends at $\phi_{max} = 320°$. Smoothing was applied at the beginning and end of the linear ramp-up motion in accord with the criteria of Eldredge *et al.* (2009). During rotation at constant velocity, the tangential velocity at the radius of gyration and at the tip were, respectively, $V_{rg} = 399$ mm s^{-1} and $V_{tip} = 618$ mm s^{-1}. Based on these values, the Reynolds number at the radius of gyration of the wing is $Re_{rg} = 15\,150$ and at the tip it is $Re_{tip} = 23\,430$.

The schematic on the right-hand side of figure 1 indicates the experimental orientation of the wing, looking toward its tip in the negative radial direction. The image orientation, also designated, is employed for all images herein.

Quantitative imaging involved an angular displacement stereo particle image velocimetry (SPIV) technique. Details of the two camera system and arrangement of liquid prisms, as well as associated uncertainties, are given in Ozen (2012). The in-plane resolution was 8.5 pixels mm^{-1}, and the field of view of the images was $4.94C \times 3.7C$, where C is the wing chord, yielding 5335 velocity vectors. Acquisition of images at a desired azimuthal angle of the plate of rotation was controlled by a computer-based system.

Extensive preliminary experiments were performed in order to determine the most representative values of rotation angle ϕ; the flow structure at the midspan was characterized for $\phi = 9°$–$270°$. Over this entire range, a stable LEV was maintained at the midspan location; no shedding of the vortex occurred. Values of $\phi = 36°$ and

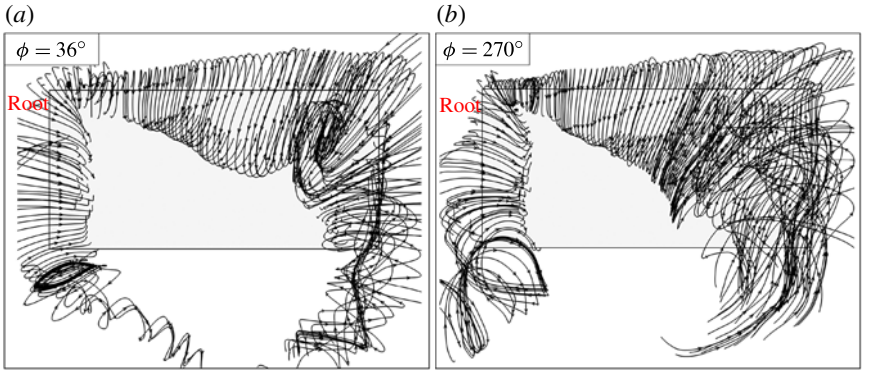

FIGURE 2. (Colour online) Three-dimensional streamline patterns for a view orthogonal to the surface of the wing (*a*) at $\phi = 36°$ and (*b*) $\phi = 270°$.

270° were selected; they correspond respectively to the passage of the wing (at its tip) through approximately $1.8C$ and $13.7C$, where C is the wing chord. At both values of ϕ, the wing rotates with constant angular velocity. Measurements and computations of Birch *et al.* (2004), Luo & Sun (2006), Poelma *et al.* (2006) and Kim & Gharib (2010) show that quasi-steady-state lift is attained prior to, or upon, passage of $4C$ to $5C$ of travel at the tip. Therefore, the limiting case of $\phi = 270°$ corresponds to attainment of the lift plateau, that is, nearly constant lift coefficient with rotation angle ϕ, and thereby a steady-state condition.

Three-dimensional phase-averaged images were constructed from ten instantaneous images acquired on each of 39 planes extending from $(r - r_o)/b = -0.097$ and to $(r - r_o)/b = 1.129$, with a spacing of $\Delta r/b = 0.032$; b denotes the span of the wing. Volume images were then reconstructed using an approach similar to Yilmaz & Rockwell (2012) for the case of a wing in rectilinear motion. The spatial separation of the velocity data on the particle image velocimetry (PIV) imaging planes is 1.89 mm corresponding to a non-dimensional distance of $\Delta x/b = \Delta y/b = 0.024$. The total number of velocity vectors in the volume corresponding to the aforementioned field of view was 208 065. The uncertainty assessment of this technique is given by Yilmaz & Rockwell (2012).

3. Three-dimensional streamline patterns

Figure 2 shows plan views of the streamline patterns on the rotating wing at two values of angle of rotation, $\phi = 36°$ and 270°. At $\phi = 36°$, a well-defined LEV along the entire span of the leading-edge is indicated by the swirl pattern of streamlines. In addition, swirl patterns occur along both the tip and root of the wing, indicating tip and root vortices. At $\phi = 270°$, the swirl pattern of streamlines associated with the LEV is well-defined up to a location of approximately 60 % span. A coherent tip vortex, of the type indicated at $\phi = 36°$, is not evident. Rather, a relatively large diameter region of non-swirling streamlines exists near the tip of the wing. At the root of the wing, a well-defined swirl pattern still exists, but in the vicinity of the trailing-edge, it takes on a complex form involving reorientation of the axis of swirl.

4. Isosurfaces of total vorticity and spanwise velocity

Figure 3(*a*) represents an isosurface of total vorticity $\omega C/V_{rg}$ at $\phi = 36°$. It indicates that the LEV is distorted as the tip of the wing is approached. The tip, root and

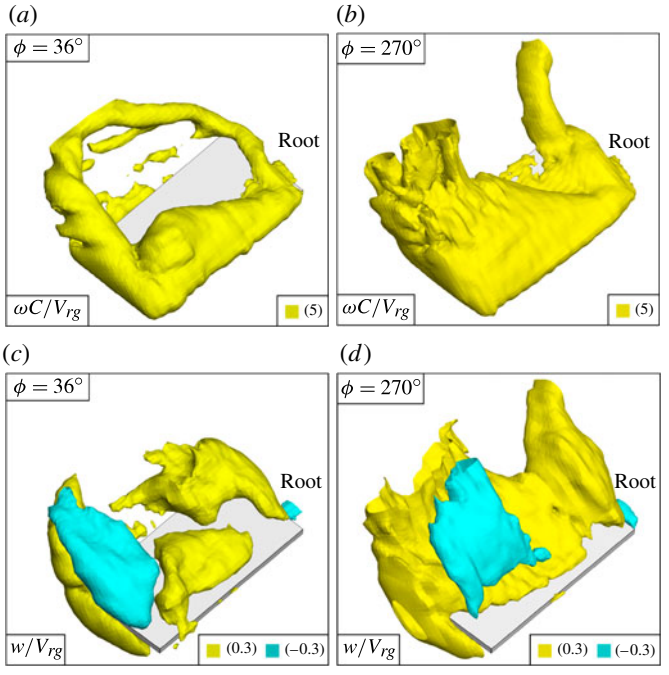

FIGURE 3. (*a*,*b*) Isosurface representations of total vorticity magnitude $\omega C/V_{rg}$ at rotation angles of $\phi = 36°$ and 270°; and (*c*,*d*) isosurfaces of spanwise velocity w/V_{rg} at $\phi = 36°$ and 270°.

trailing vortices are connected to form a loop. Also evident are small-scale vortices shed from the trailing-edge of the wing.

In figure 3(*b*), representing $\phi = 270°$, the LEV is well defined from the root to approximately 60 % span, but between the midspan and tip of the wing, it is evident that the LEV and the tip vortex have lost their identities.

Figure 3(*c*,*d*) show corresponding isosurfaces of spanwise velocity w/V_{rg}. Yellow and blue surfaces correspond respectively to positive (root to tip) and negative (tip to root) values. In figure 3(*c*), for $\phi = 36°$, positive spanwise flow from the root to the tip (yellow colour) exists along the leading-edge; it corresponds to spanwise flow through the LEV, evident by comparison with figure 3(*a*). Figure 3(*d*), representing $\phi = 270°$, indicates that the form of the isosurface of w/V_{rg} has undergone a major transformation. Positive (yellow) w/V_{rg} no longer occurs along the leading-edge. The isosurface extends along the entire span of the wing; it has a concave form and occurs predominantly in the region behind the midchord.

5. Isosurfaces of orthogonal vorticity components

Figure 4(*a–c*) show respectively isosurface representations of spanwise $\omega_z C/V_{rg}$, chordwise $\omega_x C/V_{rg}$ and normal $\omega_y C/V_{rg}$ vorticity components. As indicated in the image orientation of figure 1, the coordinate x is defined parallel to the velocity vector V_{rg} of the plate at the radius of gyration; coordinates y and z are normal to it, with z denoting the spanwise direction.

In figure 4(*a*), the forms of the isosurfaces of spanwise vorticity $\omega_z C/V_{rg}$ of the LEVs at $\phi = 36°$ and 270° have a number of features in common with the isosurfaces of total vorticity $\omega C/V_{rg}$ given in figure 3.

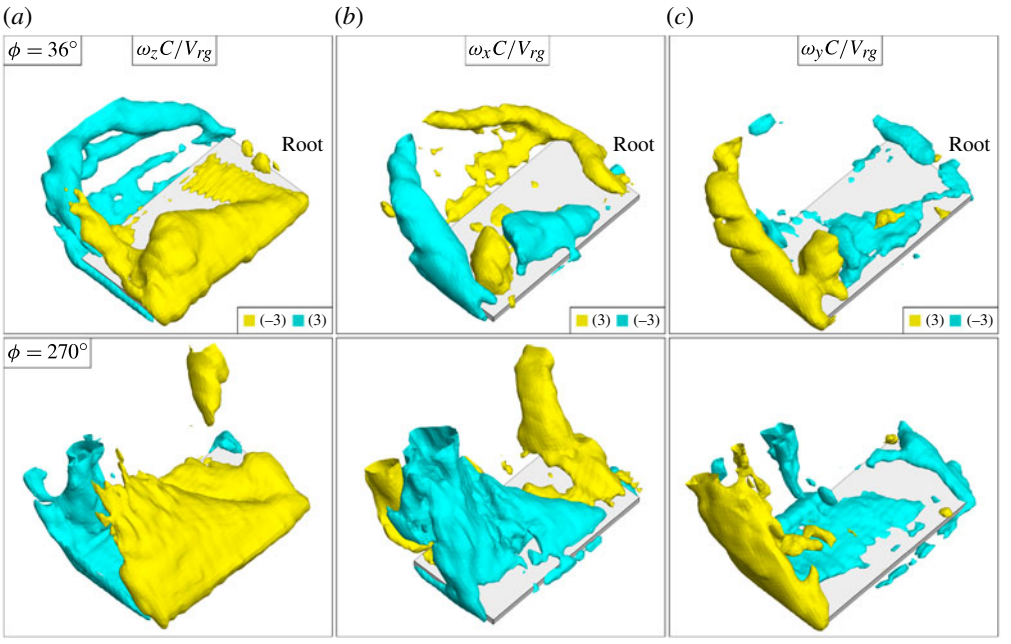

FIGURE 4. Isosurface representations of (*a*) spanwise $\omega_z C/V_{rg}$, (*b*) chordwise $\omega_x C/V_{rg}$ and (*c*) normal $\omega_y C/V_{rg}$ vorticity components at rotation angles of $\phi = 36°$ and 270°.

In figure 4(*b*), isosurfaces of negative (blue) and positive (yellow) $\omega_x C/V_{rg}$ are evident along the leading-edge. It is evident that the total vorticity isosurface at $\phi = 36°$ in figure 3(*a*) obscures the contributions of $\omega_x C/V_{rg}$ in the leading-edge region. Regarding the tip and root regions of the wing, the isosurfaces of chordwise vorticity $\omega_x C/V_{rg}$ at $\phi = 36°$ indicate that the scale of the tip vortex is substantially larger than the root vortex. At $\phi = 270°$, the isosurface of positive (yellow) $\omega_x C/V_{rg}$ no longer exists along the leading-edge; the negative (blue) $\omega_x C/V_{rg}$ isosurface persists over a portion of the leading-edge. Moreover, at the tip of the wing, a well-defined tip vortex no longer occurs, relative to tip vortex at $\phi = 36°$. On the other hand, the scale of the root vortex at $\phi = 270°$ has increased relative to that at $\phi = 36°$.

In figure 4(*c*), at $\phi = 36°$, the form of the isosurfaces of $\omega_y C/V_{rg}$ in the leading-edge region is similar to the $\omega_x C/V_{rg}$ isosurfaces of figure 4(*b*). These isosurfaces are no longer present at $\phi = 270°$.

6. Sectional cuts of flow structure: spanwise-oriented planes

Figure 5 provides a physical representation of the origin of the isosurfaces of $\omega_x C/V_{rg}$ in the leading-edge region. Images therein correspond to vertical cuts located at $x/C' = 0.29$, 0.5 and 0.71, where C' is the projection of the chord length onto the x axis. The images at the bottom of the layout of figure 5 illustrate the sectional cut (at $x/C' = 0.5$) in relation to the three-dimensional isosurfaces of $\omega_x C/V_{rg}$ at $\phi = 36°$ and 270°, taken from figure 4(*b*).

In order to provide a unified description of the chordwise evolution of the flow patterns, they are first described at the mid-chord location $x/C' = 0.5$, corresponding to the middle set of images in figure 5.

Patterns of chordwise-oriented vorticity. In figure 5, specifically the image at $\phi = 36°$, $x/C' = 0.5$, the negative (blue) tip and the positive (red–yellow) root vorticity

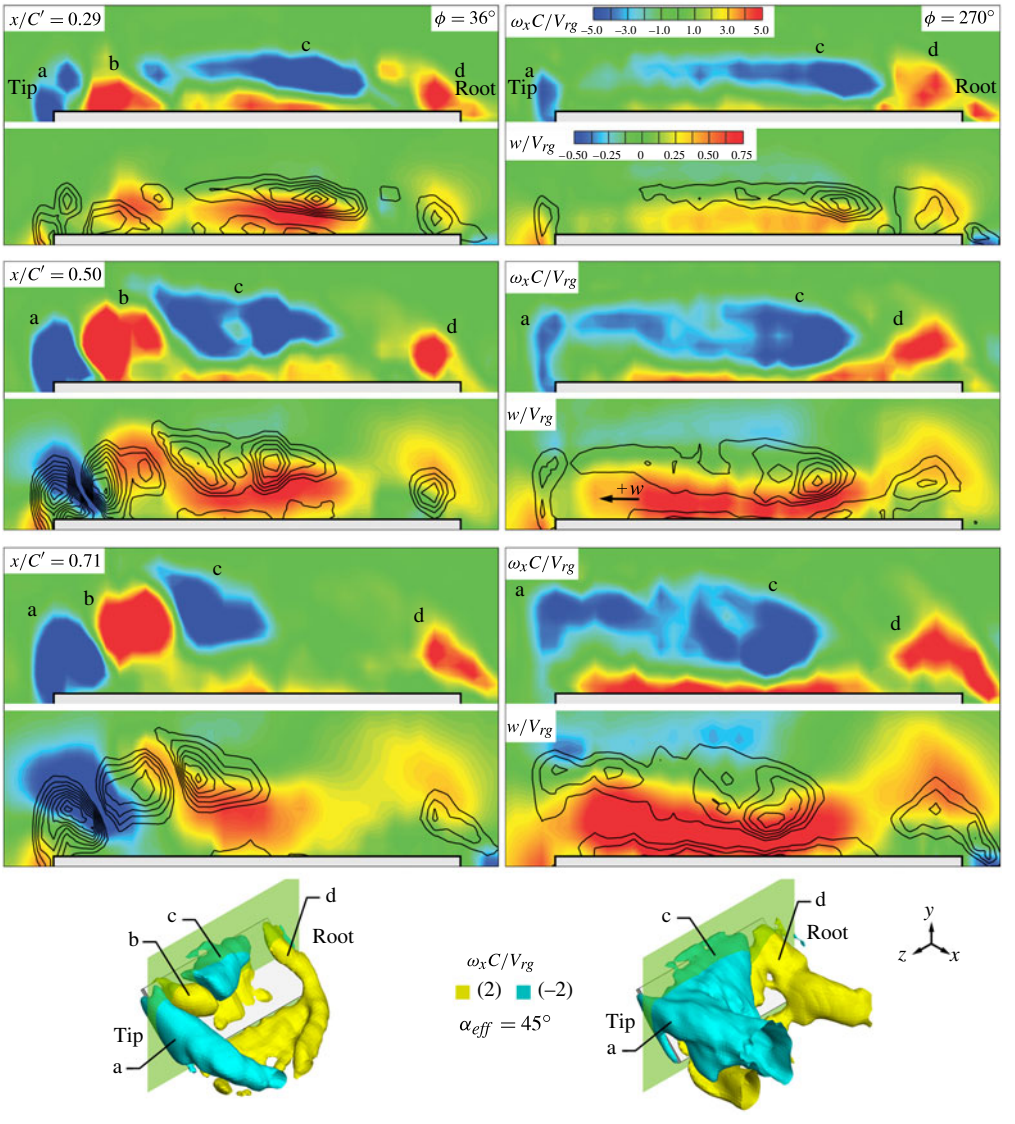

FIGURE 5. Color contours of vorticity $\omega_x C/V_{rg}$ and (black) lines of $\omega_x C/V_{rg}$ superposed on colour contours of constant spanwise velocity w/V_{rg} at streamwise locations $x/C' = 0.29$, 0.50 and 0.71 for azimuthal angles of rotation $\phi = 36°$ and 270°. Minimum and incremental values of black line contours are $(\omega_x C/V_{rg})_{min} = \pm 2.67$ and $\Delta\omega_x C/V_{rg} = 1.33$.

concentrations $\omega_x C/V_{rg}$ are designated with letters a and d. Between them, two concentrations are evident: the positive (red–yellow) concentration b due to eruption of the surface boundary layer; and the negative (blue) concentrations c, hypothesized to be due to reorientation of the spanwise vorticity of the LEV, as visualized by Ozen & Rockwell (2011) for a different mode of rotational motion of a wing; consideration of volume images of vorticity transport terms is underway and required for conclusive interpretation. In the image at $\phi = 270°$, $x/C' = 0.5$, the positive (red–yellow) concentration b is not present. The negative (blue) concentration c is

located between the root and midspan and a less concentrated region of negative (blue) vorticity $\omega_x C/V_{rg}$ extends along a substantial portion of the span to the tip vortex a.

For the images at $\phi = 36°$, $x/C' = 0.5$, the values of dimensionless circulation based on chordwise vorticity $\omega_x C/V_{rg}$ of the negative (blue) tip a and positive (red–yellow) eruption b concentrations are respectively $\Gamma_x C/V_{rg} = -0.45$ and 0.63. The corresponding value for the negative (blue) concentrations c is -0.99 and for the positive (red) root concentration d is 0.25. The vorticity concentrations b and c arising from the spanwise flow therefore have values of circulation the same order as the concentrations a and d associated with the tip and root vortices.

Patterns of spanwise velocity in relation to chordwise-oriented vorticity. The images of w/V_{rg} in figure 5 at $x/C' = 0.5$, for both $\phi = 36°$ and 270°, show the relationship between the patterns of spanwise velocity w/V_{rg} and chordwise-oriented vorticity $\omega_x C/V_{rg}$. Contours of constant w/V_{rg} are indicated in red–yellow colour, which represents positively oriented w/V_{rg} from the root to the tip of the wing; the peak magnitude of $w/V_{rg} = 0.8$. Superposed on these w/V_{rg} contours are black-line contours of constant chordwise vorticity $\omega_x C/V_{rg}$; they represent the vorticity levels of the corresponding colour contours of $\omega_x C/V_{rg}$. The maximum values of vorticity $\omega_x C/V_{rg}$ corresponding to the concentration(s) c are indicated by the black-line contours located at the outer (upper) edge of the red–yellow region of w/V_{rg}. This region has the form of a wall jet, i.e. the value of w/V_{rg} goes to zero at its outer edge. Regarding the vorticity concentration b at $\phi = 36°$, it arises from eruption of the red–yellow pattern of w/V_{rg} from the surface of the wing; this eruption occurs at a location corresponding to the red–yellow vorticity concentration b.

The basic features of the aforementioned flow patterns at the midspan $x/C' = 0.5$ are generally detectable in the images corresponding to the upstream and downstream locations $x/C' = 0.29$ and 0.71 in figure 5. A general observation is that, at both $\phi = 36°$ and 270°, the locus of the maximum negative (blue) vorticity c migrates from the root towards the tip at successively larger values of $x/C' = 0.29$, 0.5 and 0.71.

7. Sectional cuts of flow structure: chordwise-oriented planes

A traditional representation of the flow structure on a rotating wing involves one or more chordwise (x-direction)-oriented planes that show patterns of spanwise-oriented vorticity $\omega_z C/V_{rg}$. These patterns are influenced by the three-dimensionality of the flow structure described in the preceding sections.

Figure 6 compares sectional cuts at angles of rotation $\phi = 36°$ (a,c,e,g) and 270° (b,d,f,h). Seven sections along the span of the wing are indicated, including the midspan location. They are designated with letters from A to G where A is the plane closest to the root. Their locations in terms of radial distance r from the centre of rotation, in relation to the root location r_o and the span b of the wing are $(r - r_o)/b = 0.03$, 0.19, 0.34, 0.50, 0.66, 0.81 and 0.97.

Figure 6(a,b) show sectional cuts of spanwise vorticity $\omega_z C/V_{rg}$ at $\phi = 36°$ and 270°. At $\phi = 36°$ in figure 6(a), the concentrations of vorticity along the leading-edge remain compact and close to the surface of the wing. Correspondingly, in the aforementioned figure 5, at $\phi = 36°$, concentrations b and c of chordwise vorticity $\omega_x C/V_{rg}$ are located along a major share of the span of the wing.

At $\phi = 270°$ in figure 6(b), for smaller values of radial distance from the root of the wing, concentrations of $\omega_z C/V_{rg}$ are also compact and close to the surface of the wing, but for sufficiently large radial distances, the vorticity layer is elongated and deflected away from the surface. Correspondingly, in figure 5, at $\phi = 270°$, only a single concentration c of chordwise vorticity $\omega_x C/V_{rg}$ is present between the root and midspan of the wing.

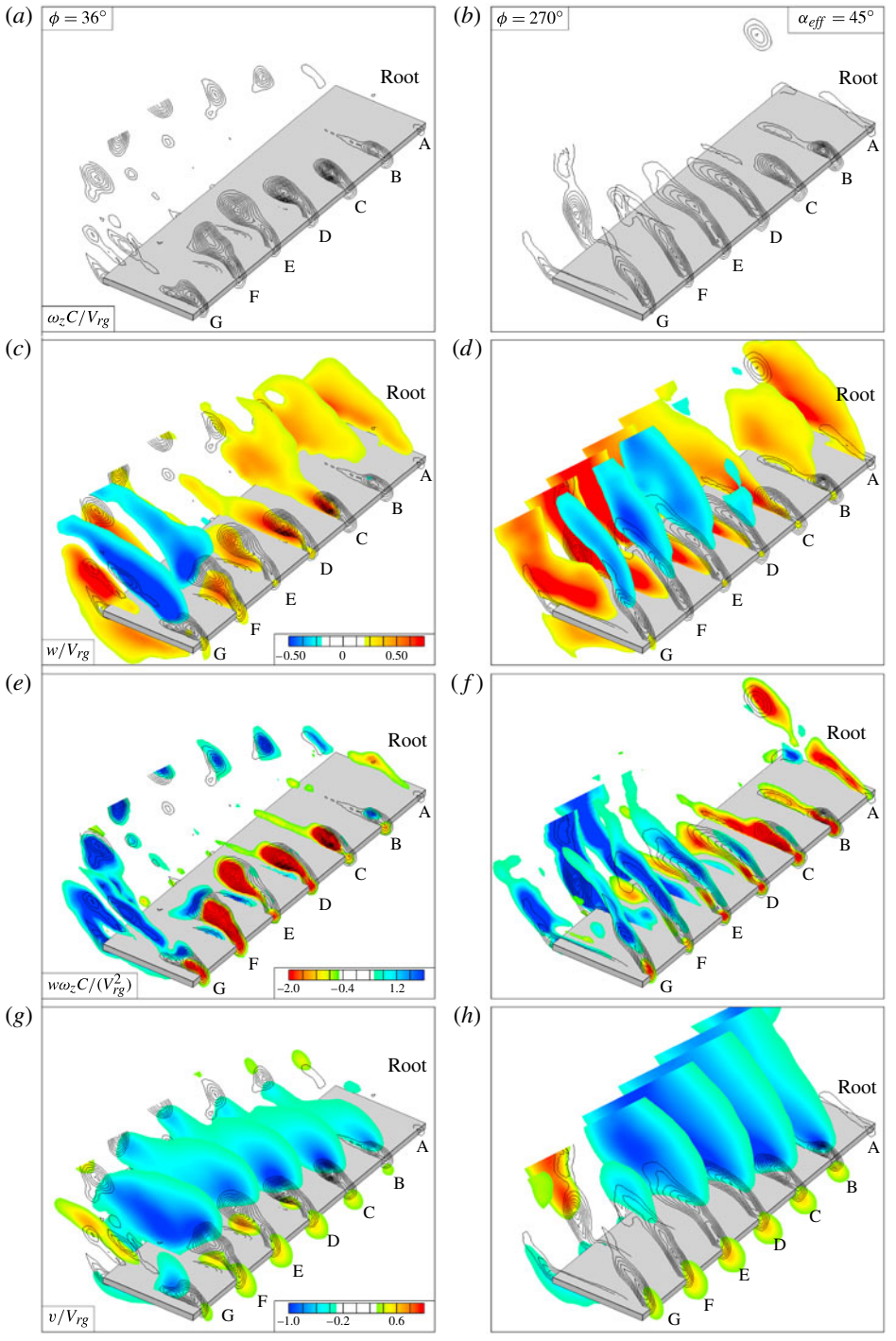

FIGURE 6. Chordwise sectional cuts of (*a*,*b*) spanwise vorticity $\omega_z C/V_{rg}$, (*c*,*d*) spanwise velocity w/V_{rg}, (*d*,*e*) spanwise vorticity flux $w\omega_z C/(V_{rg}^2)$ and (*f*,*g*) vertical (downwash) velocity v/V_{rg} at angles of rotation (*a*,*c*,*e*,*g*) $\phi = 36°$ and (*b*,*d*,*f*,*h*) $\phi = 270°$.

Figure 6(*c*,*d*) show sectional cuts of spanwise vorticity $\omega_z C/V_{rg}$ in relation to cuts of positive (red–yellow) and negative (blue) spanwise velocity w/V_{rg}. Coincidence of sufficiently large values of $\omega_z C/V_{rg}$ and w/V_{rg} yields concentrated regions of vorticity flux $w\omega_z C/(V_{rg}^2)$. Figure 6(*e*,*f*) illustrate patterns of spanwise vorticity flux $w\omega_z C/(V_{rg}^2)$ in relation to the sectional patterns of spanwise vorticity $\omega_z C/V_{rg}$. Negative (red–yellow) flux occurs at sections where the LEV is relatively concentrated and remains close to the surface, and positive (blue) flux occurs within the LEV when the vorticity layer is elongated and deflected away from the surface of the wing. The sign of vorticity flux is therefore a further indicator of the form of the sectional pattern of vorticity.

Figure 6(*g*,*h*) show sectional patterns of downwash, that is, negative (blue) v/V_{rg}. At $\phi = 36°$, downwash with values ranging from $v/V_{rg} = -0.3$ to -1.3 extend from the trailing portions of the leading-edge vorticity concentrations to the wake region; with increasing radial distance along the span, the extent of the large (dark blue) magnitude downwash becomes larger. This trend occurs in presence of increasing circulation of the LEV with radial distance, and larger circulation of the tip vortex relative to the root vortex, as indicated in figures 3–5. On the other hand, at $\phi = 270°$, the extent of large magnitude downwash decreases severely as the tip of the wing is approached at sections *E*–*G*, and correspondingly, the leading-edge vorticity layer is increasingly deflected away from the surface of the wing. This trend of loss of downwash with increasing radial distance is associated with loss of identity of the tip and LEVs at larger radial distances.

8. Conclusions

The vortex structure on a rotating wing has been characterized using an imaging technique that allows construction of volume representations. This approach provides interpretation of the three-dimensional structure of the LEV in relation to the forms of the tip and root vortices.

Existence of a coherent tip vortex is associated with identifiable concentrations of vorticity oriented in the chordwise direction (in-line with the velocity vector of the wing motion); they are located along the span of the wing. These concentrations occur in the following regions: the location of eruption of spanwise flow from the surface of the wing; and the outer edge of the spanwise flow, which has the form of a wall jet with a maximum velocity the same order as the velocity of the wing at its radius of gyration.

Loss of coherence and identity of the tip vortex is accompanied by loss of the chordwise-oriented vorticity concentration due to eruption of the spanwise flow from the wing surface, leaving a broadly distributed, lower-level region of chordwise-oriented vorticity over most of the span of the wing, and a single vorticity concentration between the root and midspan of the wing. The loss of the tip vortex is, however, accompanied by enhancement of a highly coherent root vortex.

Interpretation of the LEV in terms of sectional cuts of spanwise vorticity shows that the local scale and degree of vorticity concentration of the LEV, as well as its proximity to the surface of the wing are related to: regions of large spanwise velocity, concentrations of chordwise-oriented vorticity located along the span and downwash along the wing.

Acknowledgement

This research program was funded by the Air Force Office of Scientific Research, with Dr D. Smith as the program manager.

REFERENCES

ANSARI, S. A., PHILLIPS, N., STABLER, G., WILKINS, P. C., ZBIKOWSKI, R. & KNOWLES, K. 2009 Experimental investigation of some aspects of insect-like flapping flight aerodynamics for application to micro air vehicles. *Exp. Fluids* **46**, 777–798.

AONO, H., LIANG, F. & LIU, H. 2008 Near- and far-field aerodynamics in insect hovering flight: an integrated computational study. *J. Expl Biol.* **211**, 239–257.

BIRCH, J. M. & DICKINSON, M. H. 2001 Spanwise flow and the attachment of the leading-edge vortex on insect wings. *Nature* **412**, 729–733.

BIRCH, J. M., DICKSON, W. B. & DICKINSON, M. H. 2004 Force production and flow structure of the leading edge vortex on flapping wings at high and low Reynolds numbers. *J. Expl Biol.* **207**, 1063–1072.

CARR, Z., CHAO, C. & RINGUETTE, M. J. 2012 The effect of aspect ratio on the three-dimensional vortex formation of rotating flat-plate wings. *AIAA Paper* 2012-0912.

DEVORIA, A., MAHAJAN, P. & RINGUETTE, M. J. 2011 Vortex formation and saturation for low-aspect-ratio rotating flat plates at low Reynolds number. *AIAA Paper* 2011-396.

ELDREDGE, J. D., WANG, C. J. & OL, M. 2009 A computational study of a canonical pitch-up, pitch-down wing maneuver. *AIAA Paper* 3687.

ELLINGTON, C. P., VAN DEN BERG, C., WILLMOTT, A. P. & THOMAS, A. L. R. 1996 Leading-edge vortices in insect flight. *Nature* **384**, 626–630.

JONES, A. R., FORD, C. W. P. & BABINSKY, H. 2011 Three-dimensional effects on sliding and waving wings. *AIAA J.* **48**, 633–644.

KIM, D. & GHARIB, M. 2010 Experimental study of three-dimensional vortex structures in translating and rotating plates. *Exp. Fluids* **49**, 329–339.

LENTINK, D. & DICKINSON, M. H. 2009 Rotational accelerations stabilize leading edge vortices on revolving fly wings. *J. Expl Biol.* **212**, 2705–2719.

LIU, H., ELLINGTON, C. P., KAWACHI, K., VAN DEN BERG, C. & WILLMOTT, A. P. 1998 A computational fluid dynamic study of hawkmoth hovering. *J. Expl Biol.* **201**, 461–477.

LU, Y. & SHEN, G. X. 2008 Three-dimensional flow structures and evolution of the leading-edge vortices on a flapping wing. *J. Expl Biol.* **211**, 1221–1230.

LUO, G. & SUN, M. 2006 The effects of corrugation and wing planform on the aerodynamic force production of sweeping model insect wings. *Acta. Mechanica Sin.* **21**, 531–541.

OZEN, C. A. 2012 Unsteady flow structure on rotating and flapping wings. PhD thesis, Lehigh University, Bethlehem, PA.

OZEN, C. A. & ROCKWELL, D. 2011 Vortical structures on a flapping wing. *Exp. Fluids* **50**, 23–34.

OZEN, C. A. & ROCKWELL, D. 2012 Flow structure on a rotating plate. *Exp. Fluids* **52**, 207–223.

POELMA, C., DICKSON, W. B. & DICKINSON, M. H. 2006 Time-resolved reconstruction of the full velocity field around a dynamically-scaled flapping wing. *Exp. Fluids* **41**, 213–225.

THOMAS, A. L. R., TAYLOR, G. K., SRYGLEY, R. B., NUDDS, R. L. & BOMPHREY, R. J. 2004 Dragonfly flight: free-flight and tethered flow visualizations reveal a diverse array of unsteady lift-generating mechanisms, controlled primarily via angle of attack. *J. Expl Biol.* **207**, 4299–4323.

VAN DEN BERG, C. & ELLINGTON, C. P. 1997 The three-dimensional leading-edge vortex of a hovering model hawkmoth. *Phil. Trans. R. Soc. Lond.* B. **352**, 329–340.

WILLMOTT, A. P., ELLINGTON, C. P. & THOMAS, A. L. R. 1997 Flow visualization and unsteady aerodynamics in the flight of the hawkmoth, manduca sexta. *Phil. Trans. R. Soc. Lond.* B. **352**, 303–316.

WOJCIK, C. J. & BUCHHOLZ, J. H. J. 2012 The dynamics of spanwise vorticity on a rotating flat plate. *AIAA Paper* 2012-0915.

YILMAZ, T. O. & ROCKWELL, D. 2012 Flow structure on finite-span wings due to pitch-up motion. *J. Fluid Mech.* **691**, 518–545.